Asia-Pacific Journal of Science and Technology: Volume: 29. Issue: 02. Article ID.: APST-29-02-14. Research Article

APST

Asia-Pacific Journal of Science and Technology

https://www.tci-thaijo.org/index.php/APST/index

Published by the Research and Graduate Studies,
Khon Kaen University, Thailand

Effect of the fabrication parameters of MWCNTs/α-MnO_2 nanocomposite through the Taguchi technique

Zakir Hussain[1] and Pranjal Sarmah[2,*]

[1]Department of Mechanical Engineering, Saroj Institute of Technology & Management, Uttar Pradesh, India
[2]Department of Mechanical Engineering, Dibrugarh University, Assam, India
[*]Corresponding author: pksnit07@dibru.ac.in

Received 12 December 2023
Revised 5 March 2023
Accepted 20 March 2023

Abstract

The objective of this research was to examine the effect of powder-processing parameters on the responses: bulk mass density and microhardness of multi-walled carbon nanotubes (MWCNTs)/manganese dioxide (α-MnO_2) nanocomposite through the Taguchi technique. The impact of powder-preparing parameters on responses was examined utilizing the signal-to-noise ratio, and an analysis of variance. The production of the MWCNTs/α-MnO_2 nanocomposite was confirmed by X-ray diffraction (XRD), scanning electron microscopy, and energy-dispersive X-ray investigation. Four variables viz. wt.% loading of MWCNTs in α-MnO_2, compaction pressure, sintering temperature, and holding time were utilized in this work as powder processing parameters. The results indicated that the experiment was carried out at optimal bulk mass density with a 10 wt.% loading of MWCNTs, an 80 MPa compaction pressure, a 475°C sintering temperature, and a 15 min holding time. Similarly, the experiment was done at a 10 wt.% MWCNTs loading, an 80 MPa compaction pressure, a 500°C sintering temperature, and a 0-min holding time to obtain the optimal microhardness value of the nanocomposite. The analysis of variance shows that the effect of the wt.% loading of MWCNTs was significant in both situations. The percentage contribution of all variables to responses revealed that the wt.% loading of MWCNTs provided the highest contribution to both responses, followed by compaction pressure. Furthermore, the confirmation test revealed that the percentage errors between the estimated and experimental signal-to-noise ratios for bulk mass density and microhardness were 0.6% and 0.66%, respectively.

Keywords: Manganese dioxide, Multi-walled carbon nanotubes, Nanocomposite, Powder metallurgy, Taguchi method

1. Introduction

In the industrial sector, the need for multifunctional materials is increasing rapidly. Nanocomposites are composite materials containing at least one nanometer-sized phase that are widely employed in a variety of engineering disciplines. The multi-walled carbon nanotubes/manganese dioxide (MWCNTs/α-MnO_2) nanocomposite is frequently employed as an electrode material owing to its outstanding capacitive performance in aqueous solutions. The primary goal of the material test is to determine a material's appropriateness for certain technological applications [1]. Fewer publications have been published about the mechanical characteristics of MWCNTs/α-MnO_2 nanocomposites than their electrical characteristics. MWCNTs/MnO_2 nanocomposite production for multifunctional applications is still in its immature stage, and popularizing this nanocomposite requires a deeper comprehension of fabrication process variables. One of the most challenging issues in the fabrication of MWCNTs/MnO_2 nanocomposite is the ability to uniformly distribute MnO_2 throughout the MWCNTs. Hussein et al. studied the effect of wt.% of MWCNTs on MWCNTs/α-MnO_2 nanocomposites and found that the microhardness of nanocomposites depends on the density, nanotube weight fraction, tube orientation, and MWCNTs dispersion in H_2SO_4 solution [1]. Despite tremendous advances in nanocomposite research, the manufacturing method remains one of the most important concerns in determining component performance. The optimal powder-processing parameters are critical for the effective application of MWCNTs/α-

MnO_2 nanocomposite as a multifunctional material with simultaneous electrical, mechanical, and tribological characteristics.

The Taguchi approach provides the design engineer with an efficient approach to determining the best design parameters at the lowest feasible cost while simultaneously improving process variance [2, 3]. Hussain et al. revealed that compaction pressure, rather than sintering temperature, had a greater relationship with the mass density and hardness of MWCNTs/Al nanocomposite [4]. Hussain et al. also reported that the compaction pressure was significant when compared to other effects on the mass density and hardness of alumina/copper composite based on the Taguchi technique coupled with Grey relational analysis [5]. Ujah et al. [6] found that temperature, temperature-dwell time interaction, and temperature-heating rate interaction were the most important factors influencing the microhardness of the aluminum-carbon nanotubes-niobium nanocomposite. Hussain et al. [3] studied the best yield parameter of MWCNTs/α-MnO_2 nanocomposites and found that the concentration of the H_2SO_4 solution was the most effective parameter on the nanocomposite's yield. Ravichandran and Anandakrishnan studied the influence of compaction pressure, sintering temperature, and sintering duration on the strength coefficient of an aluminum matrix composite containing 10% molybdenum trioxide particles [7]. They concluded that the most effective factors that determine the strength coefficient were compaction pressure and sintering temperature. Chauhan et al. used a design of experiments to determine the optimal combination of process parameters for an iron-chromium-molybdenum alloy [8]. By using the Taguchi approach, Pour et al. optimized the production parameters of nano-calcium carbonate to attain the highest production rate [9]. The grey-based Taguchi technique was utilized by Navaneetha and Athijayamani to optimize the fabrication parameters, and they showed that the fiber content was the most significant parameter that impacted responses [10]. Pietrzak et al. created an alumina-copper composite material and reported that correct sintering conditions were required to maximize the composite's characteristics [11]. According to Vairamuthu et al., compaction pressure and sintering temperature had a significant impact on density and hardness [12]. However, compression strength was mostly influenced by sintering temperature and time. Alam et al. reported that titanium carbide was the most significant variable in increasing the density and microhardness of composites made of graphite and aluminum [13]. Uday et al. demonstrated that the Taguchi approach was superior to the response surface methodology for improving surface finish in wire electrical discharge machining [14].

The MWCNTs/α-MnO_2 nanocomposite is generally used for making electrodes for supercapacitors. The literature suggests that the mechanical characteristics of the MWCNTs/α-MnO_2 nanocomposite have not received much attention. Hussain et al. investigated the effect of MWCNTs wt.% on the MnO_2 matrix. They did not find the optimal parameters required to obtain the high performance of the material [1], motivating us to evaluate its performance under optimal conditions. As a result, the objective of the research is to investigate the effect of powder metallurgy processing parameters on the responses: bulk mass density and microhardness of MWCNTs/α-MnO_2 nanocomposite through the Taguchi approach.

The MWCNTs/α-MnO_2 nanocomposite was compacted using a hydraulic press machine (model: H type, make: Nitin Hydraulic and Engineering, India). In a muffle furnace, the sintering process was carried out (model: XD-1200 MST, make: Zhengzhou Brother Furnace Co. Ltd., China). An X-ray diffractometer (model: Mini Flex, brand: Rigaku, USA) using Cu-Kα radiation was used to examine the nanocomposite's crystallographic structure. A field emission scanning electron microscope (model: SIGMA VP, make: ZEISS, Germany) was used to describe the surface morphology of MWCNTs/α-MnO_2 nanocomposite. A microhardness tester (model: Micro WizHard, make: Mitutoyo, Japan) was used to conduct the microhardness tests. Minitab version 2018 statistical software was used to prepare the designs, graphs, and analyses for this investigation.

2. Materials and methods

2.1 Materials

M/S Jaya Electrical, Electronics, Scientific, Equipment & Instruments, Kolkata supplied the reinforcing material, multi-walled carbon nanotubes (make: Sisco Research Laboratory Pvt. Ltd, India, purity: >99%, Outer diameter: 30-50 nm, Length: 10-20 μm) which was prepared by the catalytic vapor deposition technique, and the oxidizing agent, $KMnO_4$ (make: EMPLURA, purity ≥98.5%). The laboratory-grade H_2SO_4 (purity: 99%) used in the study was purchased from Northeast Chemicals, India. In this article, α-MnO_2 was used as a matrix material for the synthesis of MWCNTs/α-MnO_2 nanocomposites.

2.2 Selection of parameter level and orthogonal array

A pilot study on nanocomposite materials was conducted due to a lack of information on the powder-processing parameters of MWCNTs/α-MnO_2 nanocomposites. The weight percent (wt.%) loading of MWCNTs in α-MnO_2, the compaction pressure, the sintering temperature, and the holding time were chosen as four parameters that affect the bulk mass density and microhardness of the MWCNTs/α-MnO_2 nanocomposite. The

powder processing parameters and the experiment trial's levels of consideration are shown in Table 1. For conducting trials, a mixed-level Taguchi's L_{16} orthogonal array has been used, and each row of the array represents several parameter-level combinations.

Table 1 Process parameters and their levels

Symbol	Parameter (Unit)	Level-I	Level-II	Level-III	Level-IV
A	wt.% loading of MWCNTs (wt./wt.)	5	10	15	20
B	Compaction pressure (MPa)	50	60	70	80
C	Sintering temperature (°C)	425	450	475	500
D	Holding time (min)	0	15	-	-

2.3 Sample fabrication technique

Powder metallurgy is a solid-state approach, widely used to manufacture composite materials. The process consists mainly of the synthesis of powders, mixing of powders, compaction, and sintering of green compacted samples. In this research, all trials were carried out under the level combinations. Three experiments were conducted for each trial run to evaluate the average value of each response. The nanocomposites were prepared using the powder metallurgy process [1,15-16], and the fabrication steps are discussed below.

2.3.1 Preparation of 10 wt% of powder

In this study, the reinforcing and matrix materials were MWCNTs and α-MnO_2, respectively. Chen et al. developed a unique and cost-effective approach for synthesizing α-MWCNTs/MnO_2 nanocomposite samples [1, 3,17]. Initially, 0.2 g of multi-walled carbon nanotubes were immersed in a 2 M boiling H_2SO_4 (aq) solution and stirred for 2 h using a magnetic stirrer (make: IKA, Germany). Due to the poor dispersion of MWCNTs in the boiling H_2SO_4 (aq) solution, the mixture was sonicated as shown in Figure 1(A) for 2 h in an ultrasonic bath (make: PCI Analytics, wattage: 120W). After 4 h, 4 g of potassium permanganate ($KMnO_4$) was added to the mixture at 85°C-90°C. With the addition of an oxidizing agent, the color of the solution gradually changed from purple to brown, indicating the production of MWCNTs/α-MnO_2 nanocomposite. The solution was brought to room temperature. The recovered yield was rinsed multiple times with acetone and de-ionized water before being dried in a laboratory oven at 80°C. Similarly, we fabricated 5, 15, and 20 wt.% loading of MWCNTs in MWCNTs/MnO_2 nanocomposite powder.

2.3.2 Compaction of powder

The varying wt.% loadings of MWCNTs in MnO_2 powders were compacted in a hydraulically driven pellet press machine with compaction pressures ranging from 50 MPa to 80 MPa. The samples in this processing phase are commonly referred to as green compact samples.

2.3.3 Sintering of green compacted samples

The sintering of samples was performed on a muffle furnace under various experimental circumstances. Specifically, the temperature was changed from 425°C to 500°C [18] and then maintained at this range for 0-15 min. Finally, each sample was cooled in the furnace environment. Figure 1(B) depicts sintered samples under various experimental conditions. The diameter and thickness of the samples are 14.9 mm and 2.5 mm, respectively.

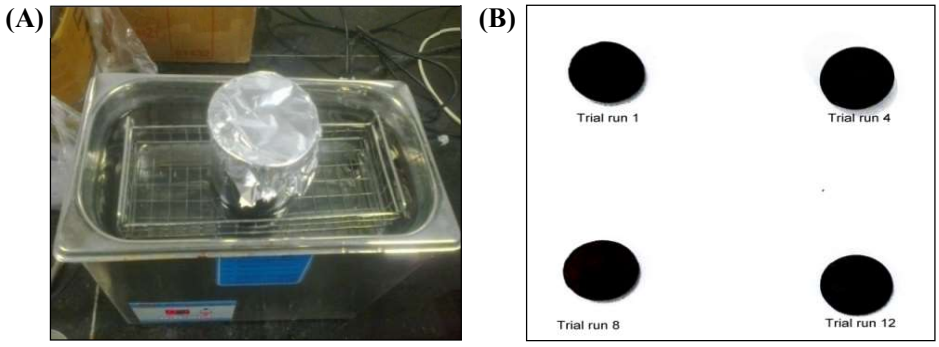

Figure 1 (A) Ultrasonic bath and (B) MWCNTs/α-MnO_2 nanocomposite at different experimental trials.

2.4 Measurement of responses

2.4.1 Measurement of bulk mass density

The experimental density of the nanocomposite samples was calculated using Archimedes' principle. The nanocomposite samples were first weighed (w_a) in air and then weighed (w_w) in distilled water. The density of water (ρ_w) was determined using the mass and volume of water contained in a cylinder. The density of materials depends on temperature. Therefore, the density of all samples was evaluated at room temperature (25°C). The experimental density of the nanocomposites was calculated using Equation (1) [19].

$$\rho_{actual} = \frac{w_a}{w_a - w_w} \times \rho_w \quad (1)$$

where ρ_{actual} is the actual density of nanocomposite, W_a is the weight of the sample in air, ρ_w is the density of distilled water and W_w is the weight of the sample in distilled water.

2.4.2 Measurement of Microhardness

The Vickers microhardness tester was used to assess the microhardness of the α-MWCNTs/MnO_2 nanocomposite. To ensure the indentation was just on the surface, the test was run with a 200-gf load at a dwell time of 30 sec. The mean indentation diagonal length was calculated for the samples after 10 repetitions of indentation for each load. Utilizing the following Equation (2), the Vickers microhardness was decided.

$$HV = 1.8544 \times \frac{P}{d_2} \quad (2)$$

where the indentation mark's mean diagonal length, d, equals ($\frac{d_1+d_2}{2}$). The indentation mark's two diagonal lengths are d_1 and d_2, respectively.

2.4.3 Evaluation of effective parameters on responses

The Taguchi technique is effectively used in single-response process optimization problems. This technique evaluates the optimal performance of a process by optimizing the condition of input variables. The effect of powder-preparation conditions on responses was investigated using Taguchi's signal-to-noise ratio and variance analysis.

3. Results and discussion

3.1 Chemical characterization

3.1.1 X-ray diffraction (XRD) pattern of MWCNTs/MnO_2 nanocomposite

The MWCNTs/α-MnO_2 nanocomposite's crystalline structure was identified using a Mini-Flex X-ray diffractometer with Cu-Kα radiation. The chemical elements of the MWCNTs/MnO_2 nanocomposites for all trial tests were the same. Therefore, the XRD of the sample was performed at 10 wt. % loading of MWCNTs in α-MnO_2, compression pressure of 80 MPa, sintering temperature of 475°C, and holding time of 0 min. Figure 2(A) depicts the XRD pattern of MWCNTs, which displays a diffraction peak at 25.69^0 and a reflection of graphite at the (002) plane [1,3,20-21]. Except for the diffraction peak of MWCNTs at 25.69^0, all other diffraction peaks may be attributed to a single-crystal, tetragonal α-MnO_2, space group: I4/m (87), as shown in Figure 2(B). The distinctive peaks of α-MnO_2 should be ascribed to additional significant intensity peaks seen on the sample at planes (110), (200), (310), (211), (301), (411), (600), (521), and (002) (JCPDS Card No. 44-0141). As a result, the XRD graph supports the synthesis of MWCNTs/α-MnO_2 nanocomposite [1,3,20-21].

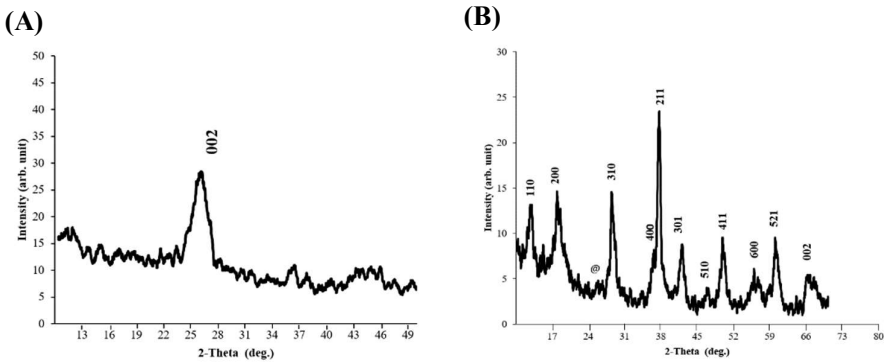

Figure 2 XRD patterns of (A) MWCNTs and (B) MWCNTs/α-MnO_2 nanocomposite.

3.1.2 Surface morphology analysis of MWCNTs/α-MnO_2 nanocomposite

A scanning electron microscope image of as-received MWCNTs is shown in Figure 3(A). The figure revealed that the MWCNTs are randomly distributed and aggregated in tangles. The tube diameter was evaluated using Image J software 1.53 a (Wayne Rasband, USA). The average diameter of MWCNTs is ~40 nm. Figure 3(B) depicts a high-resolution field emission scanning electron microscopic picture of the trial sample fabricated to a 10 wt.% loading of MWCNTs in α-MnO_2, compression pressure of 80 MPa, sintering temperature of 475^{0}C, and holding time of 0 min. According to the figure, the average diameter of MWCNTs increased from 40 nm to 198 nm, indicating a thin α-MnO_2 layer covering MWCNTs. Similar surface morphology was found for the sample fabricated at 20 wt. % loading of MWCNTs in α-MnO_2, compression pressure of 80 MPa, sintering temperature of 425^{0}C, and holding time of 0 min as depicted in Figure 3(C). Figures 3(B)-3(C) show that the α-MnO_2 is non-uniformly grown on the surface of MWCNTs and the tubes are randomly oriented. The length of the MWCNTs became short due to their oxidation by $KMnO_4$ and the ultra-sonication process of the pre-mixture [22].

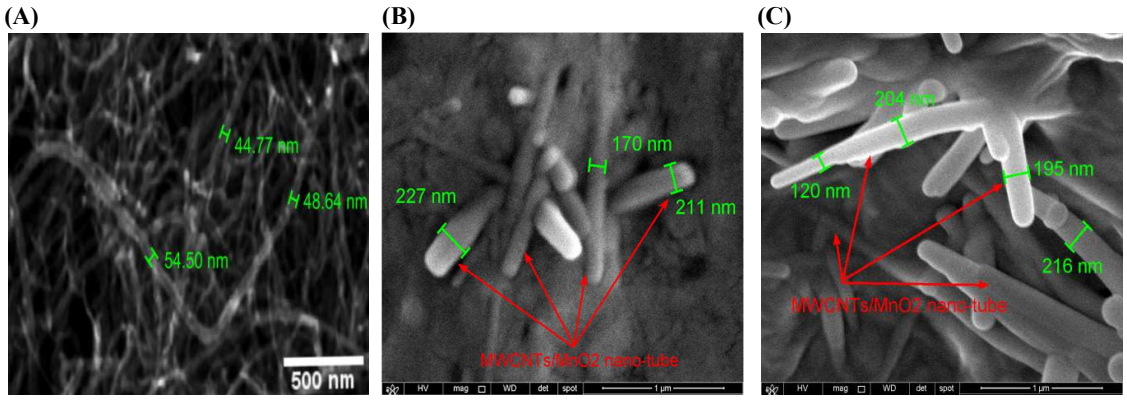

Figure 3 Surface morphology of (A) as received MWCNTs at x30,000; (B) 10 wt.% α-MWCNTs/α-MnO_2 nanocomposite under a compression pressure of 80 MPa, the sintering temperature of 475°C, and holding duration of 0 min; and (C) 20 wt.% MWCNTs/α-MnO_2 nanocomposite under a compression pressure of 80 MPa, a sintering temperature of 425°C, and a holding duration of 0 min.

3.1.3 Energy-dispersive X-Ray Analysis of 10wt% α-MWCNTs/MnO_2 nanocomposite

Figure 4 illustrates the energy-dispersive X-Ray (EDX) spectra of the 10 wt.% MWCNTs/α-MnO_2 nanocomposite. The figure reveals the presence of potassium (K) as a contaminant and the chemical elements manganese (Mn), oxygen (O), and carbon (C). The nanocomposite sample contains the chemical element C because MnO_2 exposed some portions of the MWCNTs. Therefore, the α-MnO_2 coating on the surface of MWCNTs is not homogeneous. K might be produced during the synthesis of MWCNT/α-MnO_2 powder from $KMnO_4$, which may be removed from the yield through centrifuging and washing with ethanol or combining distilled water and alcohol. Since the density of K (0.862 g/cm^3) is lower compared to the density of MWCNTs (~1.3-1.4 g/cm^3 [23]) and MnO_2 (4.63 g/cm^3 [24]). Therefore, the density of the nanocomposite decreases with the addition of K. Again, the metallic bond of potassium is weak due to the presence of one valance electron, which can effectively reduce the hardness value of the nanocomposite.

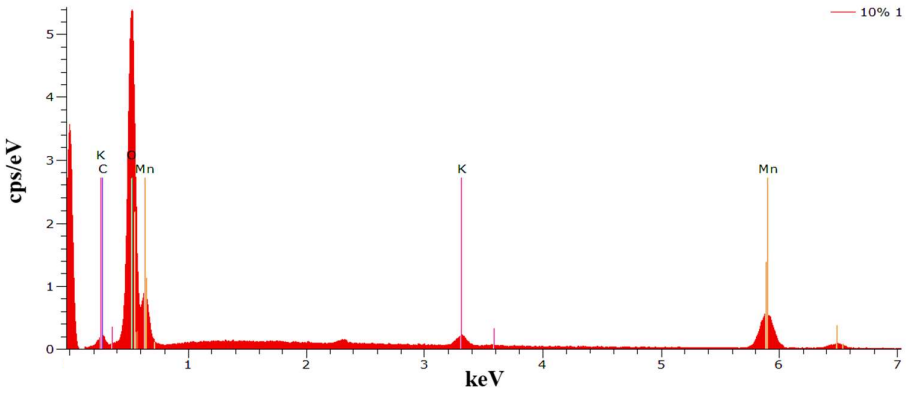

Figure 4 EDX spectrum of MWCNTs/MnO_2 nanocomposite.

3.2 Analysis of the signal-to-noise (SN) ratio

The experimental density of water is 996.2±0.83 kg/m^3 which is very close to the density of water at 25°C [5]. The density of MnO_2 may decrease due to the presence of porosity [25]. So, in the study of the bulk mass density of the nanocomposite, a "higher-the-better" criterion is chosen to find SN ratios. Again, the hardness value for the 10 wt% MWCNTs in the α-MnO_2 matrix is 38.55 kgf/mm^2 [1]. To respond to microhardness, higher-the-better criteria have been chosen.

Table 2 shows the experimental data and related SN ratios for the responses. The experimental results indicate that the responses are maximum at optimal wt. % loading MWCNTs in the MnO_2 at 10 wt.%. With increasing wt.% loading of MWCNTs above the optimal value, reduced nanocomposite properties [26]. Many researchers found that the optimum loading of MWCNTs was essential and the lower properties above the optimal wt.% of MWCNTs were due to the presence of agglomeration of MWCNTs in the nanocomposite. Hussain et al. found that the mass density and microhardness of MWCNTs/α-MnO_2 nanocomposites were highest at the 10 wt.% loading of MWCNTs [1]. Our results also suggested that the 10 wt.% of loading of MWCNTs at an optimal level increases the bulk mass density and microhardness of the MWCNTs/α-MnO_2 nanocomposite. Scanning electron microscopic images as shown in Figures 3(B-C) revealed the non-uniform growth of α-MnO_2 on the surface of MWCNTs, which can also increase the porosity in the nanocomposite. Therefore, the dispersion of MWCNTs and uniform growth of α-MnO_2 on the surface of MWCNTs have affected the performance of the nanocomposite. The bulk mass density and microhardness of the nanocomposites were also affected as compaction pressure and sintering temperature increased. Composition, compaction pressure, sintering temperature, size and form of the combined powders, and MWCNTs dispersion in the matrix all have an impact on nanocomposite characteristics [27,28]. Figure 5 displays the indentation mark left by Vickers indenter on the nanocomposite specimen. Figure 5 shows that the cracks developed at the sides, which indicates the brittle behavior of the nanocomposite. The variation of the microhardness value from the indentation mark in Figure 5(A) to the indentation mark in Figure 5(B) for the same trial run may be due to the presence of defects during the fabrication process viz. presence of impurity element, formation of pores, surface roughness, distribution of reinforcement material, or the matrix area without reinforcement material [29]. Figures 6 (A-B) show the main effect plots of the SN ratios at each level for the response variables: bulk mass density and microhardness, respectively. According to Figure 6 and response Table 3, the optimal factor level combination for density is $A_2B_4C_3D_2$, which corresponds to a wt. % loading of MWCNTs in α-MnO_2 of 10%, compression pressure of 80 MPa, sintering temperature of 475°C, and holding time of 15 min. On the other hand, the optimal factor level combination for microhardness is $A_2B_4C_4D_1$, which entails loading MWCNTs in MnO_2 at a wt.% of 10%, compression pressure of 80 MPa, the sintering temperature of 500^0C, and holding time of 0 min. Figures 6 (A-B) show that increasing compaction pressure and sintering temperature from level-1 to level-2 decreases the nanocomposite properties. This may be due to the non-uniform growth of α-MnO_2 on the surface of MWCNTs and the agglomeration of MWCNTs in the nanocomposite. The mean microhardness value of the nanocomposite from level-2 to level-3 is enhanced with increasing compaction pressure and sintering temperature due to the strong interaction between the combined materials and the shearing of load by MWCNTs on the α-MnO_2 [30]. The response Table 3 also shows that the wt.% loading of MWCNTs in α-MnO_2 is ranked 1st in the contribution of responses due to the large difference in mean SN ratio between the highest and lowest levels followed by compaction pressure, sintering temperature, and holding time. The effect of holding time is less significant compared to other main effects.

Table 2 Experimental results and SN ratios.

Sl. no.	A	B	C	D	Density (g/cm^3)	Microhardness (kgf/mm^2)	SN Ratio for density (dB)	SN Ratio for microhardness (dB)
1	5	50	425	0	2.426±0.031	30.61±1.43	7.697	29.717
2	5	60	450	0	2.340±0.026	29.37±1.36	7.383	29.358
3	5	70	475	15	2.394±0.039	30.16±1.59	7.584	29.5886
4	5	80	500	15	2.436±0.014	31.76±1.13	7.733	30.0376
5	10	50	450	15	2.655±0.029	40.26±1.37	8.481	32.097
6	10	60	425	15	2.692±0.022	41.43±1.07	8.603	32.346
7	10	70	500	0	2.755±0.034	44.22±1.87	8.802	32.912
8	10	80	475	0	2.806±0.027	45.76±1.21	8.964	33.210
9	15	50	475	0	2.284±0.017	33.37±1.49	7.174	30.467
10	15	60	500	0	2.181±0.024	34.61±1.02	6.772	30.784
11	15	70	425	15	2.246±0.031	34.16±1.39	7.031	30.670
12	15	80	450	15	2.296±0.019	35.76±1.42	7.222	31.068
13	20	50	500	15	2.232±0.038	26.78±1.06	6.973	28.556
14	20	60	475	15	2.196±0.02	24.24±1.25	6.832	27.691
15	20	70	450	0	2.136±0.011	25.5±1.54	6.595	28.131
16	20	80	425	0	2.158±0.038	28.39±1.84	6.682	29.063

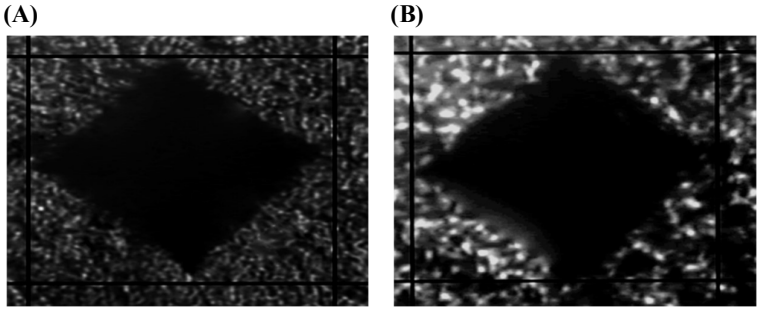

Figure 5 Indentation mark produced by indentation on nanocomposite specimen: (A) experiment 8 at 1st location; and (B) experiment 8 at 2nd location.

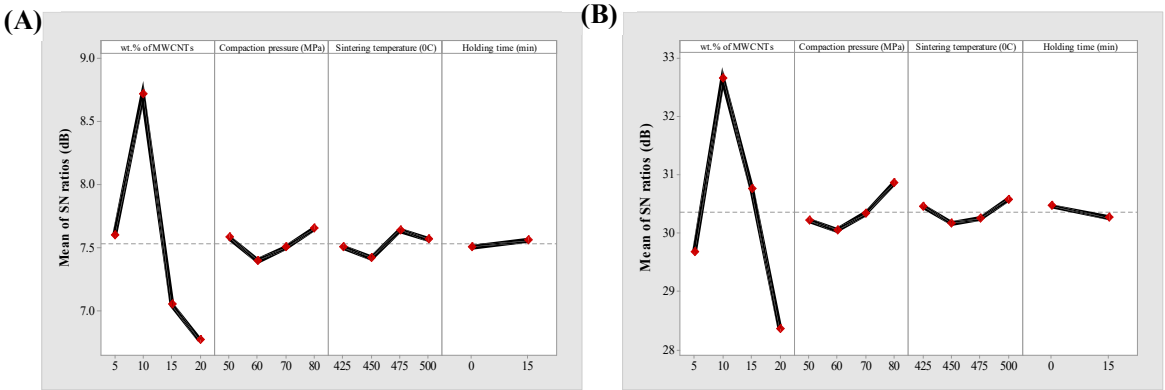

Figure 6 Main effect plots of SN ratios for (A) bulk mass density; and (B) microhardness.

Table 3 Response table for signal-to-noise ratios.

Larger-is-better (response: bulk mass density)					Larger-is-better (response: microhardness)			
Level	wt. % of MWCNTs	Compaction pressure (MPa)	Sintering temperature (^{0}C)	Holding time (min)	wt. % of MWCNTs	Compaction pressure (MPa)	Sintering temperature (^{0}C)	Holding time (min)
1	7.60	7.58	7.50	7.51	29.68	30.21	30.45	30.46
2	8.71	7.40	7.42	7.56	32.64	30.04	30.16	30.26
3	7.05	7.50	7.64		30.75	30.33	30.24	
4	6.77	7.65	7.57		28.36	30.84	30.57	
Delta	1.94	0.25	0.22	0.04	4.28	0.8	0.41	0.2
Rank	1	2	3	4	1	2	3	4

3.3 Interaction plots

The interaction plots for the SN ratios with parameters are shown in Figure 7. Since the lines are not parallel, Figures 7(A) and 7(B) illustrate the existence of an interaction impact on responses between the variables. As a result, there is compelling evidence that the factors of MWCNTs loading wt.%, compaction pressure, sintering temperature, and holding time interact to affect both responses.

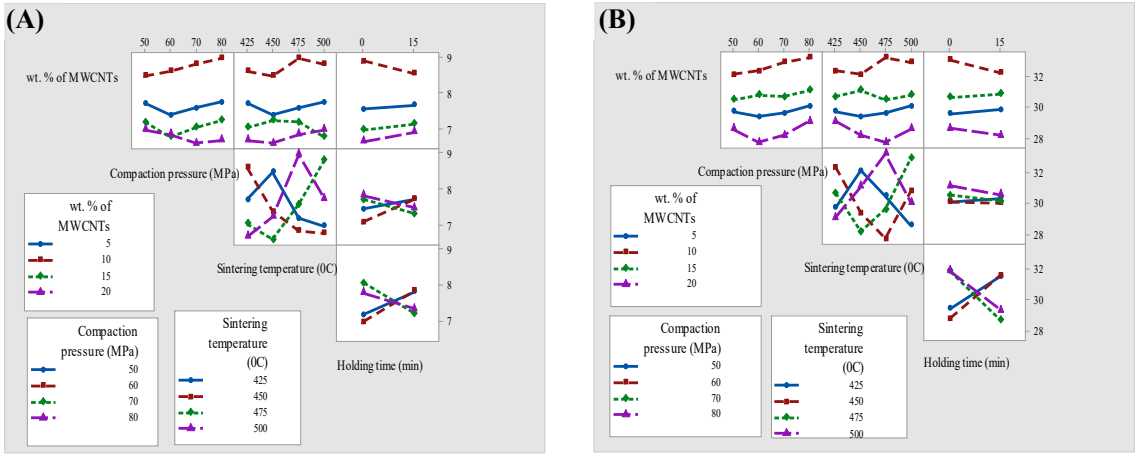

Figure 7 Interaction plots of SN ratios for response (A) bulk mass density and (B) microhardness.

3.4 Analysis of variance (ANOVA) for response

The hypotheses for the analysis are 1) Null hypothesis (H_0): powder processing parameters have an insignificant effect on the response and 2) Alternative hypothesis (H_1): powder processing parameters have a significant effect on the response.

The findings of the ANOVA table for the SN ratio of responses: bulk mass density and microhardness are shown in Tables 4 and 5, respectively. The difference at the two levels for the responses-bulk mass density and microhardness was determined to be significant at a 95% confidence interval for the wt.% loading of MWCNTs because the *p*-value was found to be less than 0.05. $p<0.05$ indicates the rejection of the null hypothesis. Therefore, we can say that the parameter affects the response. The percentage contribution of each component is further shown in Tables 5 and 6, with the wt.% of MWCNTs making the largest contributions (95.5% and 94.6%, respectively) when compared to other parameters, followed by the compaction pressure on bulk mass density and microhardness. The other variables effect is negligible in both situations. Additionally, the percentage error contributions of all variables on bulk mass density and microhardness are 1.74% and 0.548%, respectively. The R^2 values for bulk mass density and microhardness model are 0.9826 and 0.995, respectively, showing that the adopted general linear model is effective. Therefore, the interaction effects between parameters on responses are ineffective compared to the main effects. According to the investigation, the parameter with the largest influence on bulk mass density and hardness is the wt.% of MWCNTs. To maximize the performance of nanocomposites, material manufacturing parameters are the most useful factors.

Table 4 Analysis of variance table of SN ratio (response: bulk mass density).

Source	Degree of freedom (DF)	Adjusted sum of square (SS)	Adjusted mean square (MS)	F-Value	*p*-Value	% Contribution	Model Summary
A	3	8.840	2.950	91.22	0	95.50	R-sq: 98.26%
B	3	0.141	0.047	1.46	0.33	1.53	R-sq(adj): 94.77%
C	3	0.104	0.034	1.08	0.44	1.19	R-sq(pred): 82.13%
D	1	0.009	0.009	0.29	0.61	0.10	
Error	5	0.162	0.032			1.74	
Total	15	9.261				100	

Table 5 Analysis of variance table of SN ratio (response: bulk mass density).

Source	Degree of freedom (DF)	Adjusted sum of square (SS)	Adjusted mean square (MS)	F-Value	*p*-Value	% Contribution	Model Summary
A	3	39.291	13.097	287.29	0	94.6	R-sq: 99.45%
B	3	1.4321	0.4774	10.47	0.014	3.45	R-sq(adj): 98.35%
C	3	0.4252	0.1417	3.11	0.127	1.02	R-sq(pred): 94.38%
D	1	0.1575	0.1575	3.46	0.122	0.38	
Error	5	0.2279	0.0456			0.55	
Total	15	41.534				100	

Table 6 Confirmation experiment for the responses.

Optimal setting				Predicted		Experimental	
A	B	C	D	Bulk density (g/cm^3)	SN ratio (dB)	Bulk density (g/cm^3)	SN ratio (dB)
2	4	3	2	2.7964	8.96	2.823±0.017	9.014
A	B	C	D	Microhardness (kgf/mm^2)	SN ratio (dB)	Microhardness (kgf/mm^2)	SN ratio (dB)
2	4	4	1	46.1	33.44	45.81±1.26	33.22

Figure 8(A) shows the normal probability curves for the standard residues in the linear mass density model. For the linear microhardness model, Figure 8(B) shows the normal probability plot of the standard residuals. The *p*-values with a 95% confidence interval are greater than 0.05, demonstrating that the standardized residuals are normally dispersed. The model, subsequently, appears to work well.

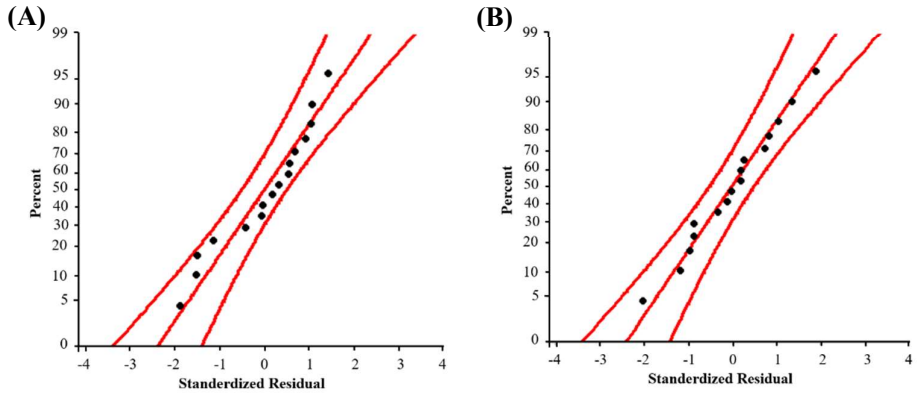

Figure 8 (A) Standard residual normal probability plot for the linear bulk mass density model; and (B) standard residual normal probability plot for the linear mass microhardness model.

3.5 Error measurement for responses

The estimated value of the SN ratio of the bulk mass density model can be evaluated using Equation (3)

$$\bar{\eta} + \left(\bar{\eta}_{A_2} - \bar{\eta}\right) + \left(\bar{\eta}_{B_4} - \bar{\eta}\right) + \left(\bar{\eta}_{C_3} - \bar{\eta}\right) + \left(\bar{\eta}_{D_2} - \bar{\eta}\right) \quad (3)$$

$\bar{\eta}$=Mean SN ratio, $\bar{\eta}_{A_2}$= Mean SN ratio at Level 2 for variable A, $\bar{\eta}_{B_4}$= Mean SN ratio at Level 4 for Variable B, $\bar{\eta}_{C_3}$= Mean SN ratio at Level 3 for Variable C and $\bar{\eta}_{D_2}$= Mean SN ratio at Level 2 for Variable D.

Similarly, the estimated value of the SN ratio of the microhardness model can be evaluated using Equation (4)

$$\bar{\eta} + \left(\bar{\eta}_{A_2} - \bar{\eta}\right) + \left(\bar{\eta}_{B_4} - \bar{\eta}\right) + \left(\bar{\eta}_{C_4} - \bar{\eta}\right) + \left(\bar{\eta}_{D_1} - \bar{\eta}\right) \quad (4)$$

Table 6 compares the estimated and confirmation experiment results utilizing the optimal level of the parameters in responses. $A_2B_4C_3D_2$ has an experimental bulk mass density of 2.823 g/cm^3 and an SN ratio of 9.014 dB at the optimum-level combination. As a result, the percentage error between the estimated and experimental SN ratio for the best-level combination is 0.6%. At its best, the $A_2B_4C_4D_1$ combination had a microhardness of 45.81 kgf/mm^2 and an SN ratio of 33.22 dB. As a result, the % error between the estimated and experimental SN ratio for the best-level combination is 0.66%.

4. Conclusion

The current study concentrated on the use of the Taguchi technique to optimize process parameters on the bulk mass density and microhardness of MWCNTs/α-MnO_2 nanocomposite. The XRD investigation demonstrates the synthesis of the MWCNTs/α-MnO_2 nanocomposite. Scanning electron microscopic image analysis revealed that the MWCNTs developed a thin α-MnO_2 layer coating. The nanocomposite contains the elements manganese, oxygen, and carbon, as evidenced by the energy-dispersive X-ray spectra. According to the mean SN ratio analysis, the experiment was carried out at a wt.% loading of MWCNTs in α-MnO_2 of 10%, compression pressure of 80 MPa, sintering temperature of 475°C, and holding time of 15 min to achieve the optimal bulk mass density. To obtain an optimal microhardness value, the experiment was carried out with a 10 wt.% loading of MWCNTs in MnO_2, compression pressure of 80 MPa, sintering temperature of 500°C, and holding time of 0 min. The ANOVA results show that the wt.% loading of MWCNTs is statistically significant, with contributions of 95.5% and 94.6% on bulk mass density and microhardness, respectively. The accuracy of the ANOVA models is high due to their higher R^2 values for bulk mass density (0.9826) and microhardness (0.995) models. Therefore, the interaction effect between variables on responses is insignificant. The confirmation test revealed that the percentage change between the estimated and actual SN ratios on bulk mass density and microhardness was 0.6% and 0.66%, respectively. The MWCNTs/α-MnO_2 nanocomposite has a bulk mass density of 2.823 g/cm^3 and a microhardness of 45.81 kgf/mm^2 at the best powder metallurgy processing settings. Therefore, the Taguchi technique improves the bulk mass density and microhardness of the nanocomposite. To maximize the performance of nanocomposites, optimization of material process parameters is the most useful factor.

5. References

[1] Hussain MZ, Khan S, Nagarajan R, Khan U, Vats V. Fabrication and microhardness analysis of MWCNT/MnO_2 nanocomposite. J Mater. 2016;2016:1-10.

[2] Taguchi G. Introduction to quality engineering: designing quality into products and processes. 9th ed. Tokyo: Asian Productivity Organization; 1986.

[3] Hussain MZ, Khan S, Gaur A, Shuaib M. Optimum yield parameters of MWCNT/MnO_2 nanocomposite, Int J Adv Res Innov. 2017;5(2):279-282.

[4] Hussain MZ, Khan S, Khan U. Optimization of MWCNTs/Al nanocomposite fabrication process parameters for mass density and hardness. Proc Inst Mech Eng C J Mech Eng Sci. 2022;236(14):8073-8091.

[5] Hussain MZ, Khan S, Sarmah P. Optimization of powder metallurgy processing parameters of Al_2O_3/Cu composite through Taguchi method with Grey relational analysis. J King Saud Univ Eng Sci. 2020;32(4):274-286.

[6] Ujah CO, Popoola API, Popoola OM, Aigbodion VS. Optimisation of spark plasma sintering parameters of Al-CNTs-Nb nano-composite using Taguchi design of experiment. Int J Adv Manuf Technol. 2019;100(5):1563-1573.

[7] Ravichandran M, Anandakrishnan V. Optimization of powder metallurgy parameters to attain maximum strength coefficient in Al-10 wt% MoO_3 composite. J Mater Res. 2015;30(15):2380-2387.

[8] Chauhan S, Verma V, Prakash U, Tewari PC, Khanduja D. Analysis of powder metallurgy process parameters for mechanical properties of sintered Fe–Cr–Mo alloy steel. Mater Manuf Process. 2017;32(5):537-541.

[9] Pour GT, Moghadam SM. Optimisation of nano-calcium carbonate production process using Taguchi method. Int J Mater Mech Manuf. 2014;2(1):77-80.

[10] Navaneethakrishnan S, Athijayamani A. Taguchi method for optimization of fabrication parameters with mechanical properties in fiber and particulate reinforced composites. Int J Plast Technol. 2015;19(2):227-240.

[11] Pietrzak K, Jach K, Kalinski D, Chmielewski M, Morgiel J. Processing and microstructure of Al_2O_3-Cu composite material interpenetrating network type. The Euro International Powder Metallurgy Congress and Exhibition (Euro PM 2011); 2011 Oct 9-12; Barcelona, Spain. Belgium: European Powder Metallurgy Association; 2011. p.1-6.

[12] Vairamuthu J, Kumar SA, Stalin B, Ravichandran M. Optimization of powder metallurgy parameters of TiC-and B4C-reinforced aluminium composites by Taguchi method. Trans Can Soc Mech Eng. 2020;45(2):249-261.

[13] Alam MA, Ya HH, Yusuf M, Sivraj R, Mamat OB, Sapuan SM, et al. Modeling, optimization and performance evaluation of TiC/graphite reinforced Al 7075 hybrid composites using response surface methodology. Materials. 2021;14(16):4703.

[14] Kandala AV, Solomon DG, Arulraj JJ. Advantages of Taguchi method compared to response surface methodology for achieving the best surface finish in wire electrical discharge machining (WEDM). J Mech Eng. 2022;19(1):185-200.

[15] Hussain MZ, Khan U, Chanda AK, Jangid R. Fabrication and hardness analysis of F-MWCNTs reinforced aluminium nanocomposite. Procedia Eng. 2017;173:1611-1618.

[16] Hussain MZ, Khan U, Jangid R, Khan S. Hardness and wear analysis of Cu/Al_2O_3 composite for application in EDM electrode. IOP Conf Ser Mater Sci Eng. 2018;310(1):012044.

[17] Chen Y, Liu CG, Liu C, Lu GQ, Cheng HM. Growth of single-crystal α-MnO_2 nanorods on multi-walled carbon nanotubes. Mater Res Bull. 2007;42(11):1935-1941.

[18] Zou MM, Ai DJ, Liu KY. Template synthesis of MnO_2/CNT nanocomposite and its application in rechargeable lithium batteries. Trans Nonferrous Met Soc China. 2011;21(9):2010-2014.

[19] Thiraviam R, Sornakumar T, Kumar SA. Development of copper: alumina metal matrix composite by powder metallurgy method. Int J Mater Prod Technol. 2008;31(2-4):305-313.

[20] Tjong SC. Carbon nanotube reinforced composites. 1st ed. Weinheim: Wiley VCH; 2009.

[21] Xia H, Wang Y, Lin J, Lu L. Hydrothermal synthesis of MnO_2/CNT nanocomposite with a CNT core/porous MnO_2 sheath hierarchy architecture for supercapacitors. Nanoscale Res Lett. 2012;7(1):1-10.

[22] Wang H, Peng C, Peng F, Yu H, Yang J. Facile synthesis of MnO_2/CNT nanocomposite and its electrochemical performance for supercapacitors. J Mater Sci Eng B. 2011;176(14):1073-1078.

[23] Wernik JM, Meguid SA. Recent developments in multifunctional nanocomposites using carbon nanotubes. Appl Mech Rev. 2010;63(5):050801.

[24] Hussain, MZ, Khan S, Sarmah P. Effect of dry sliding wear parameters on the specific wear rate of α-MnO_2-epoxy nanocomposites. Proc Inst Mech Eng C J Mech Eng Sci. 2022;237(6):1370-1392.

[25] Fraser A, Borg JP, Jordan JL, Sutherland G. Micro-mechanical behavior of Al-MnO_2-Epoxy under shock loading while incorporating the epoxy phase transition. DYMAT 2009-9th International Conferences on the Mechanical and Physical Behaviour of Materials under Dynamic Loading; 2009 Sept 7-11; Brussels, Belgium. Paris: EDP Sciences; 2009. p.1575-1582.

[26] Tanabi H, Erdal M. Effect of CNTs dispersion on electrical, mechanical and strain sensing properties of CNT/epoxy nanocomposites. Results Phys. 2019;12:486-503.

[27] Meignanamoorthy M, Ravichandran M, Mohanavel V, Afzal A, Sathish T, Alamri S, et al. Microstructure, mechanical properties, and corrosion behavior of Boron carbide reinforced aluminum alloy (Al-Fe-Si-Zn-Cu) matrix composites produced via powder metallurgy route. Materials. 2021;14(15):4315.

[28] Trinh VP, Luan VN, Minh PN, Phuong DD. Effect of sintering temperature on properties of CNT/Al composite prepared by capsule-free hot isostatic pressing technique. Trans Indian Inst Met. 2017;70:947-955.

[29] Campo M, Suárez JA, Ureña A. Effect of type, percentage and dispersion method of multi-walled carbon nanotubes on tribological properties of epoxy composites. Wear. 2015;324-325:100-108.

[30] Carneiro Í, Simões S. Strengthening mechanisms in carbon nanotubes reinforced metal matrix composites: a review. Metals. 2021;11:1613.